Efficient lasing in continuous wave and graphene Q-switched regimes from Nd:YAG ridge waveguides produced by combination of swift heavy ion irradiation and femtosecond laser ablation

Yuechen Jia,[1] Yang Tan,[1] Chen Cheng,[1] Javier R. Vázquez de Aldana,[2] and Feng Chen[1,*]

[1]*School of Physics, Key Laboratory of Particle Physics and Particle Irradiation (Ministry of Education), and State Key Laboratory of Crystal Materials, Shandong University, Jinan 250100, China*
[2]*Laser Microprocessing Group, Universidad de Salamanca, Salamanca 37008, Spain*
[*]*drfchen@sdu.edu.cn*

Abstract: We report on the continuous wave and passively Q-switched lasers in Nd:YAG ridge waveguides fabricated by a combination of swift Kr ion irradiation and femtosecond laser ablation. Owing to the deep penetration length (~50 μm) of 670 MeV Kr^{8+} ions into the crystal, ridge waveguides with large-area cross section, supporting nearly symmetric guiding modes, were produced. Continuous wave lasers with maximum 182 mW output power at ~1064 nm have been realized at 808-nm optical pump. Using graphene as a saturable absorber, passively Q-switched waveguide laser operations were achieved. The pulsed laser produces 90 ns pulses, with a ~4.2 MHz repetition rate, 19% slope efficiency and 110 mW average output power, corresponding to single-pulse energy of 26.5 nJ.

OCIS codes: (230.7370) Waveguides; (140.3540) Lasers, Q-switched; (160.3380) Laser materials.

References and links

1. Y. N. Billeh, M. Liu, and T. Buma, "Spectroscopic photoacoustic microscopy using a photonic crystal fiber supercontinuum source," Opt. Express **18**(18), 18519–18524 (2010).
2. D. Bauer, I. Zawischa, D. H. Sutter, A. Killi, and T. Dekorsy, "Mode-locked Yb:YAG thin-disk oscillator with 41 μJ pulse energy at 145 W average infrared power and high power frequency conversion," Opt. Express **20**(9), 9698–9704 (2012).
3. R. Osellame, G. Cerullo, and R. Ramponi, *Femtosecond Laser Micromachining: Photonic and Microfluidic Devices in Transparent Materials* (Springer-Verlag, 2012).
4. J. Liu, J. Dai, S. L. Chin, and X. C. Zhang, "Broadband terahertz wave remote sensing using coherent manipulation of fluorescence from asymmetrically ionized gases," Nat. Photonics **4**(9), 627–631 (2010).
5. W. J. Cao, H. Y. Wang, A. P. Luo, Z. C. Luo, and W. C. Xu, "Graphene-based, 50 nm wide-band tunable passively Q-switched fiber laser," Laser Phys. Lett. **9**(1), 54–58 (2012).
6. V. K. Singh and A. K. Rai, "Prospects for laser-induced breakdown spectroscopy for biomedical applications: a review," Lasers Med. Sci. **26**(5), 673–687 (2011).
7. M. Laroche, A. M. Chardon, J. Nilsson, D. P. Shepherd, W. A. Clarkson, S. Girard, and R. Moncorgé, "Compact diode-pumped passively Q-switched tunable Er-Yb double-clad fiber laser," Opt. Lett. **27**(22), 1980–1982 (2002).
8. J. H. Lin, K. H. Lin, H. H. Hsu, and W. F. Hsieh, "Q-switched and mode-locked pulses generation in Nd:$GdVO_4$ laser with dual loss-modulation mechanism," Laser Phys. Lett. **5**(4), 276–280 (2008).
9. S. V. Garnov, S. A. Solokhin, E. D. Pbraztsova, A. S. Lobach, P. A. Obraztsov, A. I. Chernov, V. V. Bukin, A. A. Sirotkin, Y. D. Zagumennyi, Y. D. Zavartsev, S. A. Kutovoi, and I. A. Shcherbakov, "Passive mode-locking with carbon nanotube saturable absorber in Nd:$GdVO_4$ and Nd:$Y_{0.9}Gd_{0.1}VO_4$ lasers operating at 1.34 μm," Laser Phys. Lett. **4**(9), 648–651 (2007).
10. U. Keller, "Recent developments in compact ultrafast lasers," Nature **424**(6950), 831–838 (2003).
11. Z. Luo, M. Zhou, J. Weng, G. Huang, H. Xu, C. Ye, and Z. Cai, "Graphene-based passively Q-switched dual-wavelength erbium-doped fiber laser," Opt. Lett. **35**(21), 3709–3711 (2010).

#209507 - $15.00 USD Received 3 Apr 2014; revised 9 May 2014; accepted 13 May 2014; published 20 May 2014

12. K. S. Novoselov, A. K. Geim, S. V. Morozov, D. Jiang, Y. Zhang, S. V. Dubonos, I. V. Grigorieva, and A. A. Firsov, "Electric field effect in atomically thin carbon films," Science **306**(5696), 666–669 (2004).
13. Q. L. Bao, H. Zhang, Y. Wang, Z. H. Ni, Y. L. Yan, Z. X. Shen, K. P. Loh, and D. Y. Tang, "Atomic-layer graphene as a saturable absorber for ultrafast pulsed lasers," Adv. Funct. Mater. **19**(19), 3077–3083 (2009).
14. F. Bonaccorso, Z. Sun, T. Hasan, and A. C. Ferrari, "Graphene Photonics and Optoelectronics," Nat. Photonics **4**(9), 611–622 (2010).
15. Z. Sun, D. Popa, T. Hasan, F. Torrisi, F. Wang, E. Kelleher, J. Travers, V. Nicolosi, and A. Ferrari, "A stable,wideband tunable, near transform-limited, graphene-mode-locked, ultrafast laser," Nano Res. **3**(9), 653–660 (2010).
16. H. Zhang, Q. L. Bao, D. Y. Tang, L. M. Zhao, and K. P. Loh, "Large energy soliton erbium-doped fiber laser with a graphene-polymer composite mode locker," Appl. Phys. Lett. **95**(14), 141103 (2009).
17. H. Zhang, D. Y. Tang, L. M. Zhao, Q. L. Bao, and K. P. Loh, "Large energy mode locking of an erbium-doped fiber laser with atomic layer graphene," Opt. Express **17**(20), 17630–17635 (2009).
18. Y. W. Song, S. Y. Jang, W. S. Han, and M. K. Bae, "Graphene mode-lockers for fiber lasers functioned with evanescent field interaction," Appl. Phys. Lett. **96**(5), 051122 (2010).
19. J. I. Mackenzie, "Dielectric solid-state planar waveguide lasers: a review," IEEE J. Sel. Top. Quantum Electron. **13**(3), 626–637 (2007).
20. C. Grivas, "Optically pumped planar waveguide lasers, Part I: Fundamentals and fabrication techniques," Prog. Quantum Electron. **35**(6), 159–239 (2011).
21. J. W. Kim, S. Y. Choi, D. I. Yeom, S. Aravazhi, M. Pollnau, U. Griebner, V. Petrov, and F. Rotermund, "Yb:KYW planar waveguide laser Q-switched by evanescent-field interaction with carbon nanotubes," Opt. Lett. **38**(23), 5090–5093 (2013).
22. D. G. Lancaster, S. Gross, A. Fuerbach, H. E. Heidepriem, T. M. Monro, and M. J. Withford, "Versatile large-mode-area femtosecond laser-written Tm:ZBLAN glass chip lasers," Opt. Express **20**(25), 27503–27509 (2012).
23. R. Salas-Montiel, L. Bastard, G. Grosa, and J.-E. Broquin, "Hybrid Neodymium-doped passively Q-switched waveguide laser," Mater. Sci. Eng. B **149**(2), 181–184 (2008).
24. M. Pollnau, Y. E. Romanyuk, F. Gardillou, C. N. Borca, U. Griebner, S. Rivier, and V. Petrov, "Double Tungstate Lasers: From Bulk Toward On-Chip Integrated Waveguide Devices," IEEE J. Sel. Top. Quantum Electron. **13**(3), 661–671 (2007).
25. Y. Tan, Q. Luan, F. Liu, F. Chen, and J. R. Vázquez de Aldana, "Q-switched pulse laser generation from double-cladding Nd:YAG ceramics waveguides," Opt. Express **21**(16), 18963–18968 (2013).
26. Y. Tan, S. Akhmadaliev, S. Zhou, S. Sun, and F. Chen, "Guided continuous-wave and graphene-based Q-switched lasers in carbon ion irradiated Nd:YAG ceramic channel waveguide," Opt. Express **22**(3), 3572–3577 (2014).
27. I. Chartier, B. Ferrand, D. Pelenc, S. J. Field, D. C. Hanna, A. C. Large, D. P. Shepherd, and A. C. Tropper, "Growth and low-threshold laser oscillation of an epitaxially grown Nd:YAG waveguide," Opt. Lett. **17**(11), 810–812 (1992).
28. F. Chen, "Micro-and submicrometric waveguiding structures in optical crystals produced by ion beams for photonic applications," Laser Photon. Rev. **6**(5), 622–640 (2012).
29. D. Jauqe, F. Chen, and Y. Tan, "Scanning confocal fluorescence imaging and micro-Raman investigations of oxygen implanted channel waveguides in Nd:MgO:$LiNbO_3$," Appl. Phys. Lett. **92**(16), 161908 (2008).
30. F. Chen, Y. Tan, and D. Jaque, "Ion-implanted optical channel waveguides in neodymium-doped yttrium aluminum garnet transparent ceramics for integrated laser generation," Opt. Lett. **34**(1), 28–30 (2009).
31. F. Chen and J. R. Vázquez de Aldana, "Optical waveguides in crystalline dielectric materials produced by femtosecond-laser micromachining," Laser Photonics Rev. **8**(2), 251–275 (2014).
32. G. Lifante, *Integrated Photonics: Fundamentals* (John Wiley and Sons Ltd, 2003).
33. Y. Jia, N. Dong, F. Chen, J. R. Vázquez de Aldana, Sh. Akhmadaliev, and S. Zhou, "Ridge waveguide lasers in Nd:GGG crystals produced by swift carbon ion irradiation and femtosecond laser ablation," Opt. Express **20**(9), 9763–9768 (2012).
34. Y. Jia, N. Dong, F. Chen, J. R. Vázquez de Aldana, Sh. Akhmadaliev, and S. Zhou, "Continuous wave ridge waveguide lasers in femtosecond laser micromachined ion irradiated Nd:YAG single crystals," Opt. Mater. Express **2**(5), 657–662 (2012).
35. J. R. Vázquez de Aldana, C. Méndez, and L. Roso, "Saturation of ablation channels micro-machined in fused silica with many femtosecond laser pulses," Opt. Express **14**(3), 1329–1338 (2006).
36. A. Zoubir, L. Sha, K. Richardson, and M. Richardson, "Practical uses of femtosecond laser micro-materials processing," Appl. Phys., A Mater. Sci. Process. **77**, 311–315 (2003).
37. J. F. Ziegler, computer code, SRIM, *http://www.srim.org*.
38. J. Siebenmorgen, T. Calmano, K. Petermann, and G. Huber, "Highly efficient Yb:YAG channel waveguide laser written with a femtosecond-laser," Opt. Express **18**(15), 16035–16041 (2010).
39. D. Yevick and W. Bardyszewski, "Correspondence of variational finite-difference (relaxation) and imaginary-distance propagation methods for modal analysis," Opt. Lett. **17**(5), 329–330 (1992).
40. G. Torchia, A. Ródenas, A. Benayas, E. Cantelar, L. Roso, and D. Jaque, "Highly efficient laser action in femtosecond-written Nd: yttrium aluminum garnet ceramic waveguides," Appl. Phys. Lett. **92**(11), 111103 (2008).
41. N. Pavel, G. Salamu, F. Voicu, F. Jipa, M. Zamfirescu, and T. Dascalu, "Efficient laser emission in diode-pumped Nd:YAG buried waveguides realized by direct femtosecond-laser writing," Laser Phys. Lett. **10**(9), 095802 (2013).

#209507 - $15.00 USD Received 3 Apr 2014; revised 9 May 2014; accepted 13 May 2014; published 20 May 2014

42. R. Degl'Innocenti, S. Reidt, A. Guarino, D. Rezzonico, G. Poberaj, and P. Günter, "Micromachining of ridge optical waveguides on top of He^+-implanted β-BaB_2O_4 crystals by femtosecond laser ablation," J. Appl. Phys. **100**, 113121 (2006).
43. H. Sun, F. He, Z. Zhou, Y. Cheng, Z. Xu, K. Sugioka, and K. Midorikawa, "Fabrication of microfluidic optical waveguides on glass chips with femtosecond laser pulses," Opt. Lett. **32**(11), 1536–1538 (2007).

1. Introduction

Compact pulsed lasers are significant to address demands for a variety of applications, ranging from spectroscopy, nonlinear frequency conversion and laser processing, to remote sensing, communication and medicine [1–6]. The Q-switching is one of the dominant techniques for the pulsed laser generation. For passively pulse operation, generally a saturable absorber (SA) is required to initiate and sustain the pulsing operation against continuous wave (CW) operation in a laser. A number of materials could be emerged as SAs for the passively Q-switching, such as transition metal-doped crystals, semiconductor saturable absorber mirrors (SESAMs) and single-wall carbon nanotubes (SWNTs) [7–9]. The use of doped crystals as SAs requires extra elements (mirrors, lenses) to focus the fiber output into the crystal [7], and SESAMs have complex fabrication and packaging as well as limited bandwidth [10]. In addition, the SWNT has problems of a low damage threshold, poor stability, and poor long-term reliability [11].

Graphene, a two-dimensional material composed of a single layer of carbon atoms, has attracted tremendous attention since it was discovered by Novoselov *et al.* in 2004 [12]. Owing to the outstanding saturable absorption, graphene has been emerged as promising SAs for various photonic applications, which proposed firstly by Bao *et al.* in 2009 [13]. Compare to traditional SAs, i.e. doped bulk crystals and SESAMs, graphene features broadband operation, low-cost and ease of fabrication [14,15]. Benefiting from its unique energy band properties with the Pauli blocking principle, graphene also possesses significant advantages over SWNTs, including much lower saturation intensity, higher damage threshold, larger saturable-absorption modulation depth, ultrafast recovery time, and an ultrabroad wavelength-independent saturable-absorption range (300–2500 nm) [11,13,16–18]. Thus, graphene is an ideal alternative for ultra-broadband SAs.

Pulsed lasers based on waveguide platforms as gain media permit compact cavity design with high beam quality and high optical intensities [19–23], which are intriguing light sources for on-chip integration [24]. Employing graphene as SAs, passively Q-switched waveguide lasers have been realized in neodymium doped yttrium aluminum garnet (Nd:$Y_3Al_5O_{12}$ or Nd:YAG) ceramics [25, 26]. As one of the mostly used gain media for solid state lasers, the Nd:YAG laser crystal has deployed to a number of applications owing to its excellent fluorescence, physical and thermal properties. Waveguide lasers have been realized in Nd:YAG crystals in the systems manufactured by epitaxial growth technique [27], ion beam implantation/irradiation [28–30] and femtosecond (fs) laser inscription [31]. Compared with planar or slab (one dimensional, 1D) waveguides, the two-dimensional (2D) (in channel or ridge configurations) waveguides can restrict the light propagation in two dimensions, reaching higher optical density, and are more easily to fabricate compact integrated devices [32]. Recently, the combination of ion implantation/irradiation and femtosecond (fs) laser micromachining method has been regarded as an effective and powerful method to fabricate 2D ridge optical guiding structures (so-called Type IV configuration) [31]. Swift heavy ion irradiation (i.e., with energy higher than 1 MeV/amu) becomes an intriguing technique because relatively thick waveguides (up to tens of microns) could be produced by high-energy ion beams with ultralow fluences ($<10^{12}$ ions/cm^2) [28]. The larger dimensions of these thick waveguides may result in more efficient pump into the guided channels, and hence the considerable increment of output powers of the waveguide lasers. So far, ridge waveguide lasers in CW regime have been realized in Nd:GGG and Nd:YAG crystals utilizing the approach as mentioned above [33, 34].

In this work, we report on the lasing characteristics in both CW and graphene Q-switched regimes of a 50 × 50 μm^2 cross sectional Nd:YAG ridge waveguide, fabricated by the

#209507 - $15.00 USD Received 3 Apr 2014; revised 9 May 2014; accepted 13 May 2014; published 20 May 2014

combination of 670 MeV krypton (Kr^{8+}) ion irradiation and fs laser ablation, supporting guided laser modes with nearly symmetric distribution.

2. Experiments in details

The Nd:YAG crystal sample (doped by 1 at. % Nd^{3+} ions) used in this work was cut into wafers with dimensions of 10 × 5 × 2 mm^3 and optically polished. To obtain ridge structures, in the first step, Kr^{8+} ions at energy of 670 MeV and fluence of 2 × 10^{14} ions/cm^2 were irradiated on one samples surface (10 × 5 mm^2) to form a planar waveguide layer at the Heavy Ion Research Facility in Lanzhou (HIRFL) at the Institute of Modern Physics, Chinese Academy of Sciences. The beam direction was tilted by 7° off the sample surface normal plane to minimize channeling effect, and the ion current density was kept at a low level to avoid the heating and charging of the samples. As a result, a waveguide layer with a thickness of nearly 50 μm was constructed on the sample near-surface region. Secondly, we used a Ti:Sapphire laser system, which delivered 120 fs pulses, linearly polarized at 800 nm and with a repletion rate of 1 kHz, to fabricate the ridge structures on top of the irradiated surface (i.e., the planar waveguide layer). The laser beam was focused by a 20 × microscope objective (N.A. = 0.4), and the sample was located at a three-dimensional motorized stage with a spatial resolution of 0.2 μm. In order to get ablation grooves with depths exceeding 50 μm and with crater walls as vertical as possible, we adopted a multi-scan strategy and a large pulse energy (10 μJ) was set. For this pulse energy and our focusing conditions the estimated peak fluence was ~500 J/cm^2, which is much larger than the typical ultrafast ablation thresholds for transparent dielectrics (a few J/cm^2) meaning that we are processing deeply in the strong ablation regime: this is a way to circumvent the saturation effect of the ablation craters [35, 36]. The focus of the beam was placed at the surface of the planar waveguide layer. Under these conditions the sample was scanned at a translation velocity of 50 μm/s, corresponds to a spatial overlap between consecutive pulses of 89%. Firstly, four parallel scans were done along the sample with a lateral separation of 2 μm between consecutive scans. After that, the focus of the beam was placed at the bottom of the produced groove (~30 μm under the sample surface) and two additional scans were done at the center of the groove with a lateral separation of 4 μm. The result was an ablation channel with large aspect ratio. The fabrication procedure was repeated to produce an additional channel with a separation of 50 μm from the first one, which is similar to the thickness of the planar waveguide. With the lateral confinement of microstructured grooves (the fs-laser damaged Nd:YAG part) and vertical restriction of Kr ion irradiated planar waveguide, the 10-mm long ridge waveguide was produced on the surface of the Nd:YAG crystal. The inset in Fig. 1 shows the microphotograph of the waveguide cross section.

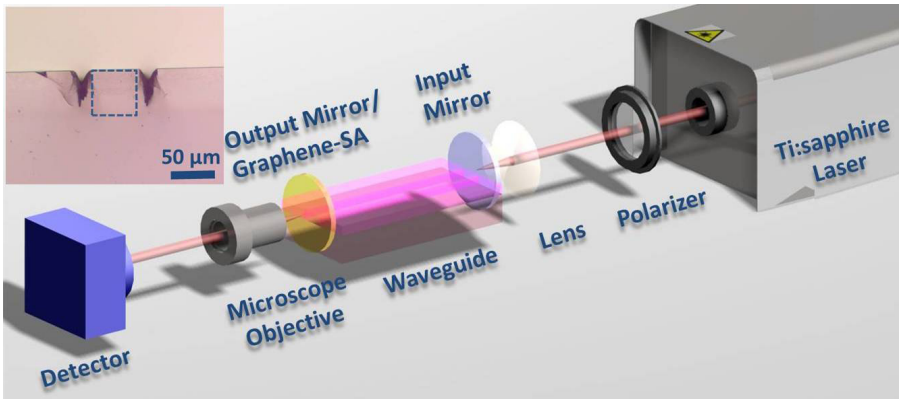

Fig. 1. Schematic plot of the experimental setup for the CW and pulse laser oscillation in the Nd:YAG ridge waveguide. The inset picture is the microphotograph of the cross section of the waveguide sample: the ridge waveguide is located in the dashed square region.

#209507 - $15.00 USD Received 3 Apr 2014; revised 9 May 2014; accepted 13 May 2014; published 20 May 2014

The waveguide laser operation experiments in CW and pulsed regimes were both performed by utilizing an end pumping system. A polarized light beam at a wavelength of 808 nm was generated from a tunable cw Ti:Sapphire laser (Coherent MBR 110) at room temperature. A convex lens with focus length of 25 mm was used to couple the laser beam into the ridge waveguide; the radius of the incident pump laser beam is approximately 0.75 mm. For the Q-switched waveguide pulsed laser generation, an input mirror (with the transmission of 98% at 808 nm and the reflectivity >99% at ~1064 nm) and a graphene film (~16 layers) coated another Nd:YAG crystal substrate as a SA, were adhered to the input and output end face of the waveguide respectively, constructing the Fabry-Perot lasing resonant cavity. Here, a set of mechanical bindings were employed to make sure the SA was closely attached to the output facet of the waveguide sample. The graphene film coated Nd:YAG substrate was provided by XFNANO Materials Tech Co., Ltd, Nanjing, China. The graphene film was grown by chemical vapor deposition (CVD) on copper and nickel firstly, with 16 layers measured by the Raman spectroscopy, and it was transferred to a transparent Nd:YAG crystal bulk with a thickness of ~2 mm. The transmission of the graphene film coated Nd:YAG crystal plate was measured to be:70% in the wavelength of 1064 nm. For the CW waveguide laser systems, the SA was replaced by an output mirror (with the reflectivity >99% at 808 nm and 60% at ~1064 nm, respectively). The generated waveguide lasers were collected by utilizing a 20 × microscope objective lens (numerical aperture N.A. = 0.4) and imaged by using an infrared CCD. We used a spectrometer with resolution of 0.2 nm to analyze the emission spectra of the laser beam from the waveguide. The schematic plot of the experimental setup for the CW and pulsed laser oscillations are depicted in Fig. 1. To investigate the attenuations of fabricated planar and ridge waveguides at the laser emission wavelength, another end coupling system was utilized, in which a CW 1064 nm laser was used as a light source. During this experiment, polarized laser beam at 1064 nm was coupled into and out of the waveguides directly without any mirror. By detecting the incident and output powers, the insertion losses of the planar and ridge waveguides were measured to be 1.2 and 2.3 dB, respectively. The higher attenuation for ridge structure should be partly attributed to the non-perfect side-walls fabricated by the fs lasers. The roughness of the side walls was estimated to be 2-4 μm by the SEM investigation.

3. Results and discussion

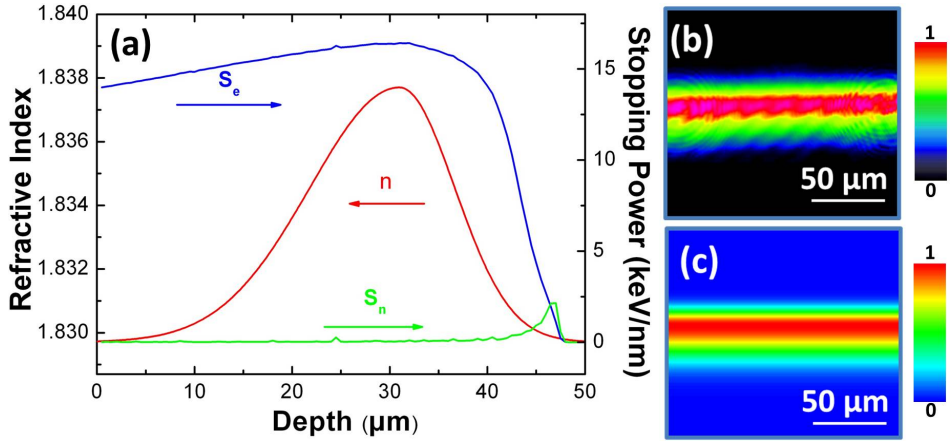

Fig. 2. (a) The electronic stopping power (blue line), nuclear stopping power (green line) curves as well as the refractive index profile (red line) of the 670 MeV Kr irradiated Nd:YAG planar waveguide as a function of the depth from the sample surface. The obtained (b) experimental and (c) simulated near-field intensity distributions of planar waveguide at 1064 nm.

#209507 - $15.00 USD Received 3 Apr 2014; revised 9 May 2014; accepted 13 May 2014; published 20 May 2014

The energy deposition process of 670MeV Kr ions irradiation on Nd:YAG crystal was simulated by the Stopping and Range of Ions in Matter (SRIM) 2010 code [37]. To investigate the modification of the ion irradiated region of the sample, we calculated the nuclear and electronic stopping power profiles, as shown in Fig. 2. From the figure, we can find that the nuclear stopping power S_n to be practically absent within the range (0-45) μm, climbing to only ~2.5 keV/nm at a depth of ~47 μm. In the case of electronic stopping power, the significantly higher value of S_e increases from the sample surface to a broad maximum at approximately ~32 μm beneath, peaking at about 17.5 keV/nm. Therefore, it is evident to suppose that the electronic damage is the major factor contributing to the formation of the waveguide layer, which is quite similar to the previously reported swift-heavy ion-irradiated Nd:YAG and Nd:GGG ridge and planar waveguides [30, 31]. By assumption of a step-like refractive index profile and measurement of the N.A. of the waveguide, we can estimate the refractive index change of the waveguide to be $\Delta n \approx + 0.008$ using the formula [38]

$$\Delta n = \frac{\sin^2 \Theta_m}{2n} \tag{1}$$

where Θ_m is the maximum incident angular deflection at which no transmitted power change is occurring, while n is the refractive index of the unmodified substrate. Thus, by combining this maximum refractive index change value with the electronic stopping power profile, we could reconstruct the refractive index distribution of the planar waveguide, as shown in Fig. 2(a). Then, based on this refractive index profile, the simulated modal distribution (Fig. 2(c)) of the waveguide was obtained by utilizing the finite-difference beam propagation (FD-BPM) method (Rsoft BeamProp 8.0) [39. By comparing the experimental and simulated near-field modal profiles in Figs. 2(b) and 2(c), one can easily conclude that there is a fairly good agreement between the experimental and simulated modal data.

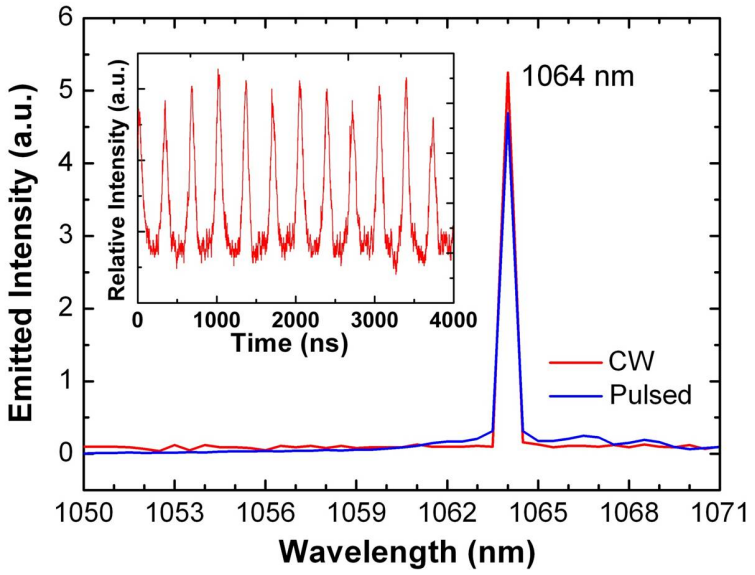

Fig. 3. Laser emission spectra from the Nd:YAG ridge waveguide in CW and graphene-SA Q-switched regimes. The inset shows the pulse train of the Q-switched waveguide laser.

Figure 3 depicts the laser emission spectrum from Nd:YAG ridge waveguide in both CW and graphene-SA Q-switched regimes at room temperature, when the absorbed pumping power is above the oscillation threshold. The central wavelengths for the CW and Q-switched pulsed ridge waveguide lasers are both ~1064 nm, which clearly denote the laser oscillation line that corresponds to the main fluorescence of $^4F_{3/2} \rightarrow {}^4I_{11/2}$ transition of Nd^{3+} ions, the full width at half maximum (FWHM) value of this spectrum is about 0.5 nm. The inset shows

#209507 - $15.00 USD Received 3 Apr 2014; revised 9 May 2014; accepted 13 May 2014; published 20 May 2014

typical oscilloscope traces of the Q-switched pulse trains under the pumping power of 535mW. The bandwidth of the oscilloscope is 200 MHz and the minimum resolution of the detector is 0.7 ns. In this case, the average output power of the pulsed laser was 42 mW. The corresponding Q-switched single-pulse energy was 14nJ with 99 ns pulse duration and 2.9 MHz pulse repetition. By varying the pumping power, the repetition rate of the ridge waveguide pulsed laser could be tuned from 0.9 MHz to 4.2 MHz (as depicted in Fig. 4(a)), when the pumping power increased from 270 mW to 850 mW. The variation of repetition rate with increasing launched pumping power is a typical and reasonable phenomenon in passively Q-switched pulsed lasers due to the strong dependence of the repetition rate on the transition rate of gain and the intracavity intensity.

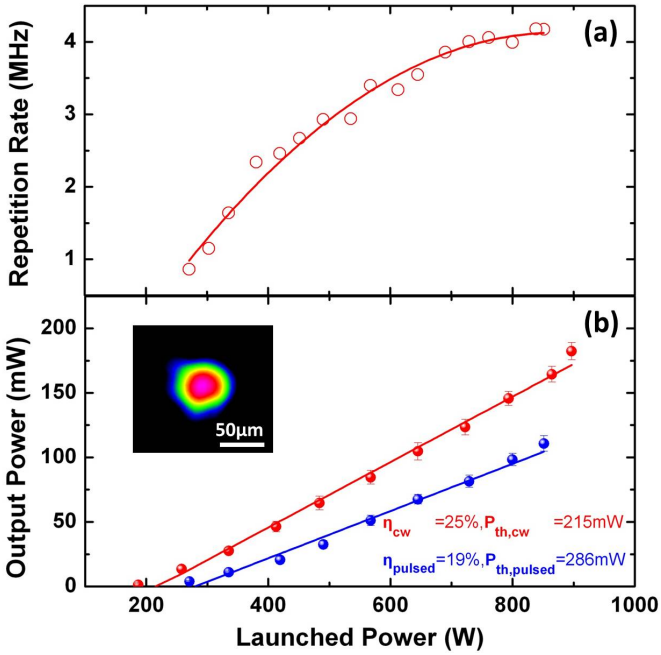

Fig. 4. (a) Repetition rate of the Q-switched waveguide laser and (b) output waveguide laser powers as a function of the launched pump in CW and Q-switched pulsed regimes. The inset depicts the laser modal profile at lasing wavelength of ~1064 nm.

Figure 4(b) illustrates the average output powers of Nd:YAG 1064-nm ridge waveguide lasers as function of launched pump power at 808 nm for CW and graphene based Q-switched configurations, employing a general output mirror and a graphene coated SA, respectively. From the linear fit of the experimental data, we have determined that the slope efficiency (η) and lasing threshold (P_{th}) of the CW (pulsed) output laser are 215 mW (286 mW) and 25% (19%). As the launched pump power increases, the CW and pulsed output laser powers climb to maximums at 182 mW and 111 mW with launched pump powers of 896 mW and 851 mW, corresponding to optical conversion efficiencies of 20% and 13%, respectively. It should be pointed out that the maximum output power of 182 mW is the largest value for any reported ion irradiated waveguide laser systems, which is about 7-8 times higher comparing to the previous CW ridge waveguide lasers in similar constructions (the maximum output powers are 25.6 and 21 mW for Nd:GGG and Nd:YAG ridge waveguide lasers, respectively) [33, 34]. This mainly benefits from the large pump volumes, resulting in remarkable enhancement of output powers. Nevertheless, in consequence of a reduction of optical intensities in waveguide configurations with large volumes, the pumping threshold would be elevated to a certain level (the CW lasing threshold of 215 mW in this work is 3-5 times higher than previous works [33, 34]). The mode intensity profile with good symmetry of the ridge waveguides shows superior features over those of most ion irradiated waveguide lasers [28].

#209507 - $15.00 USD Received 3 Apr 2014; revised 9 May 2014; accepted 13 May 2014; published 20 May 2014

In addition, it is worth to mention that the ridge waveguide lasers in the present work exhibit little difference on the polarization (the laser output power changes by only 5% when the polarization of the pump laser is rotated), which is partly due to the symmetric cross sections of the ridge waveguide structure (50 × 50 μm^2). This polarization-independent feature of the waveguide lasing in the present Nd:YAG ridge waveguide system is significantly different from the fs-laser inscribed dual-line Nd:YAG ceramic waveguides, in which only TM polarization (parallel to the damage tracks) could be well guided [40]. However, this property is similar to fs-laser written cladding Nd:YAG waveguide lasers, which operate on both TE and TM polarizations [41].

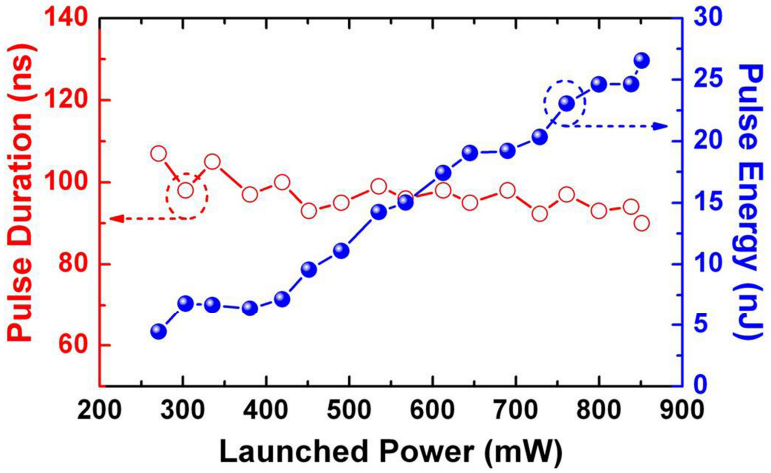

Fig. 5. Q-switched pulse duration and single-pulse energy as a function of launched pump power.

The dependences of the pulse duration and the single pulse energy versus launched pump power are indicated in Fig. 5. With the increasing of pump power, the pulse duration values present downtrend on the whole in spite of the existence of some fluctuations, varying from 104 ns near the lasing threshold to 90 ns at pump power of 851 mW. Meanwhile, the single pulse energy increases from ~4.5 nJ to ~26.5 nJ. The peak power of the output pulse is up to 0.3 kW. For passively Q-switched laser, the pulse duration could be theoretically modeled as the equation below

$$\Delta R \approx \frac{3.52 T_R}{\tau_p} \tag{2}$$

where ΔR is the modulation depth of the saturable absorber; τ_p is the pulse duration; T_R is the cavity round-trip time. Considering about the waveguide length of ~1 cm, the maximum modulation depth was calculated to be less than 1% in this work.

Finally, the waveguide lasing performance could be further optimized by reducing the guiding losses produced by fs-laser ablation induced rough sidewalls, usually post-ablation treatment (such as ion-beam sputtering) may be performed to reduce the roughness of the ablated air gaps [42]. In addition, by using multiple scans, the roughness of the sidewalls might be reduced to a certain extent [43].

4. Summary

In conclusion, the CW and graphene based Q-switched pulsed ridge waveguide lasers with nearly symmetric mode profiles at 1064 nm have been demonstrated in Nd:YAG crystal fabricated by combining swift Kr ion irradiation and fs laser micromachining. The maximum output power of 182 mW was obtained in the CW regime. The pulsed waveguide laser has a

#209507 - $15.00 USD Received 3 Apr 2014; revised 9 May 2014; accepted 13 May 2014; published 20 May 2014

range of repetition rate from 0.9 MHz to 4.2 MHz, with pulse energy of up to 26.5 nJ and pulse duration of 90 ns at pump power of 851 mW.

Acknowledgments

The work was supported by the National Natural Science Foundation of China (No. U1332121) and the 973 Project (No. 2010CB832906) of China, and Junta de Castilla y León under project SA086A12-2.

#209507 - $15.00 USD Received 3 Apr 2014; revised 9 May 2014; accepted 13 May 2014; published 20 May 2014